THE ASTROPHYSICAL JOURNAL, 205:172–181, 1976 April 1

SHOCK-WAVE INTERPRETATION OF EMISSION LINES IN LONG-PERIOD VARIABLE STARS. I. THE VELOCITY OF THE SHOCK

L. A. WILLSON*
Erwin W. Fick Observatory, Department of Physics, Iowa State University
Received 1975 June 12; revised 1975 September 18

ABSTRACT

The emission lines seen in long-period variables are classified according to the mechanism by which they are formed. This leads to information on the physical conditions in several regions, and especially to an estimate of the velocity differences between regions. The results are interpreted in terms of a spherical shock wave expanding outward at $v \approx 50$ km s^{-1} and gradually decelerating. This high shock velocity in turn implies substantial mass loss and mechanical energy output. This also implies that (*a*) mechanical energy dominates in determining the atmospheric structure and (*b*) the atmosphere is extended and spherical geometry must be used.

Subject headings: shock waves — stars: emission-line — stars: long-period variables

I. INTRODUCTION

In this paper we interpret the emission-line spectrum of long-period variables (LPVs) in the postmaximum phase in terms of a spherically symmetric shock wave propagating outward through the star's atmosphere, in an effort to determine parameters of the shock—velocity, temperature, and density—as a function of phase.

The emission lines which appear in the postmaximum spectra of long-period variables can be classified according to the process leading to their formation. For the purposes of this paper we shall assume that all the emission lines arise as a consequence of the passage of the shock wave, and thus are formed near the shock and reflect only the properties of the regions immediately behind or ahead of the shock. The principal classes of lines are then: primary lines of ionized elements, primary lines of neutral elements, and secondary "pumped" or "fluorescent" lines of neutral elements. The primary ultraviolet lines of Mg II λλ2795, 2802, and presumably the ultraviolet lines of Fe II and Ti II also, are assumed to be formed in the region immediately behind the shock, where excitation, ionization, and outward velocity are maximum. The primary lines of neutral elements, including the hydrogen Balmer series, Si I λλ3905, 4103, Fe I multiplets (2) and (3), and Mg I multiplet (3), are probably formed by thermal or recombination processes behind the shock front. The secondary, pumped, or fluorescent lines are formed ahead of the shock. They are produced by selective excitation by primary lines due to a wavelength coincidence between one of the primary lines and a transition in the neutral atom. The fluorescent lines thus fall naturally into two subclasses, depending on which class of primary lines the exciting line belongs to. A third subclass, lines pumped by other fluorescent lines, has no definite representatives on these spectra; however, Merrill (1947) mentions that Ga I multiplet (1) λ4172 pumped by λ4033 of Mn I is present in χ Cyg.

The fluorescent lines are found to contain information on the velocity discontinuity across the shock front, Δv. Velocity differences are required because the wavelength coincidences are not exact; excited transition and exciting line differ by up to 1 Å, corresponding to on the order of 100 km s^{-1}. The two subclasses of lines yield different results for the velocity difference—possibly implying a different origin for the two classes of primary lines.

From an analysis of the behavior of the first group of fluorescent lines with phase we derive a "most probable" Δv as a function of time. This gives an estimate for the magnitude of the velocity with which the shock propagates through the star's atmosphere, but not a detailed time dependence. An analysis of the widths of the hydrogen lines, however, gives an indication of the time dependence of the shock velocity, although it gives only a very poor estimate for its magnitude. The line widths may be fitted with

$$v = v_0(r/r_0)^{-\alpha}, \tag{1}$$

where v_0, the velocity at $t = 0$, is set by the fluorescent lines to be ~ 70 km s^{-1}. Several (r_0, α) pairs are possible—from $\alpha = 1$, $r_0 = 10^{13}$ cm, to $\alpha \geq 3/2$, $r_0 = 2 \times 10^{14}$ cm—and these correspond to models with different physical assumptions.

In the last section some of the implications of the high velocity indicated by the fluorescent lines are explored. It is found that the shock contributes significantly to the total luminosity of the star, and that it dominates in determining the atmospheric structure.

* Work performed in part during the summer of 1974 at the Astronomy Department, University of Washington, Seattle.

TABLE 1

EMISSION LINES IN LPV SPECTRA

A. PRIMARY LINES, FORMED IN THE REGION BEHIND THE SHOCK

Line(s)	Strength	Comment
Mg II λ2795	Strong	Presumed strong + broad
λ2802	Strong	
Ca II λ3933	?	Not seen due to overlying absorption
λ3969	?	
Fe II, Ti II ultraviolet lines	...	Presumed present
Fe II multiplets (2), (3) and (28)	...	Intensities and widths anomalous; overlying absorption?
Ti II multiplets (11), (13)	...	

B. HYDROGEN-LIKE LINES

Line(s)	Strength	Width	Comment
H Balmer lines	Strong!	$\lesssim 100$ km s^{-1}	
Si I λ4103, 3905	Strong	$\lesssim 60$ km s^{-1}	Vary like H lines
Mg I multiplet (3)	Moderate	$\lesssim 40$ km s^{-1}	
Fe I multiplet (2), (3)	Weak	$\lesssim 40$ km s^{-1}	(Including absorption)
Fe I multiplet (18)–(20)	Weak	< 40 km s^{-1}	

C. FLUORESCENT LINES (pumped lines)

ΔV(km s^{-1})*	λ exciter	Multiplet + λ_{seen}	χ_l	χ_u	I/I_{comp}	Max. Phase (days)	Comments
		a) Excited by Mg II, Ca II, Fe II, Ti II					
−2	2795 Mg II	Fe I (50), (118), ...	0.91	5.33	...	...	Not seen
+3	3121 Ti II	Co I (32) 3935	0.10	4.05	Strong; blended	0	Not likely†
+22	3933 Ca I	Sc I (8) 3907	0.02	3.16	$\gtrsim 200$	100	Strong
+25	2802 Mg II	Ti I (277) 4372	0.90	5.30	No comp.	180	
+56	2795 Mg II	Fe I (42) 4202	0.00	4.42	25	135	Lines very strong
+62	3072 Ti II	Co I (32) 3997	0.17	4.19	~1	40	< λ3935
+70	2620 Fe II	Ti I (86) 3789	0.05	4.76	~1	...	? Unidentified in MAS‡
+76	2795 Mg II	Mn (2) 4030, 33, 34	0.00	4.42	No comp.	+90	Indirect pumping
+88	2795 Mg II	Fe I (73) 3852	0.95	5.37	35	+80	Affected by 4202 strength
+95	2913 Ti II	Fe I (21) 3758, ...	0.00	4.24	...	...	Not pumped
+174	2802 Mg II	Mn I (2) 4030, 33, 34	0.00	4.41	No comp.	+90	Not likely
		b) Excited by H					
−30	4101 Hδ	V I (41) 4119	1.05	4.06	≤4	...	Possibly present
−14	3835 H9	V I (44) 3844	1.04	4.26	25	...	Present
−2	4101 Hδ	In I (1) 4511	0.00	3.01	No comp.	...	Present, medium
+41	3889 H8	Fe I (45) 3827	1.60	4.77	≤1	...	Not significantly enhanced
+61	3970 Hε	Fe I (43) 4063	*1.48**	4.59	~10	70	Dep. on 4202 pump
		c) Excited by Neutral Metals					
0	4291 Fe I	Fe I (41) 4294	*1.55*	4.43	40	...	
+8	3017 Fe I	Co I (32) 3997	0.10	...	~1	...	Or by Ti II
+32	4033 Mn I	Fe I (44)	*1.48*	...	≤2	...	No enhancement
+32	4045 Fe I	Co I (31)	1.04	...	4	...	?
+42	4030 Mn I	Fe I (72) 4001	2.19	5.25	2	...	Probably not pumped
+74	2529 Fe I	Si I (2) 4103	0.03	4.91	No comp.	0	Probably not pumped
+123	3475 Fe I	Co I (16) 4058	0.00	3.55	≤5	...	Not likely
+123	3475 Fe I	Co I (16) 4058	0.00	3.55	≤5	...	Not likely

NOTE.—Italicized entries mean that the level is overpopulated as a result of another coincidence.

* Positive Δv means exciting atom is *approaching* region where pumped line is formed. This sense is used because it transforms to positive outward velocities of the shock region in the model.

† Co I λ3935 behaves in all respects as though it is pumped by a strong line like λλ2795, 2802, with $\Delta v \equiv 60$–100 km s^{-1}, although no exciter has been found despite lengthy searching. If it is assumed to be pumped this way, the rest of the Co I lines seen are easily explained in the same manner as, e.g., λ4063 of Fe I. If λ3121 Ti II were responsible, then Co I λ3997 pumped by λ3072 Ti II should be stronger than λ3935, rather than weaker.

‡ Meinel, Aveni, and Stockton 1969.

Observational material used for this analysis included recent plates of R Leo and R Aql at 4.4 and 6.0 Å mm^{-1} taken by G. Wallerstein at Dominion Astrophysical Observatory, and some earlier 2.8–10.2 Å mm^{-1} plates from Hale Observatories files.

II. CLASSIFICATION OF THE EMISSION LINES

In order to study the structure of the shock wave using the emission lines, one must first elucidate where in relation to the shock the lines are formed. A first step forward this goal is classifying the lines according to their width or shape and to the mechanism whereby they are formed. Such a classification is summarized in Table 1.

The first class of lines, presumably formed in the hottest region immediately behind the shock, are the ultraviolet lines of singly ionized elements—Mg II, Fe II, Ti II, etc. The strongest of these are the Mg II lines at 2795, 2802 Å. These emission lines have been observed in Betelgeuse (see Kondo *et al.* 1972) and in Arcturus (Moos *et al.* 1974) where they are strong and broad, even though visible emission in secondary lines is not seen. They should be even stronger in the long-period variables, and it is thus not surprising that they give rise to many strong secondary lines. For the purposes of this paper we need not further investigate the nature of the Mg II emission lines; it is sufficient to assume that they are formed (*a*) in a region moving outward with approximately the velocity of the shock front and (*b*) with a width at the point of their formation that is sufficient to account for all the secondary lines which are seen. The stronger Fe II and Ti II lines in the ultraviolet are also assumed present, formed in the shock. Some visible emission lines of Fe II and Ti II can be seen in the stellar spectra also; however, their profiles are of uncertain width and irregular form, probably due to absorption by overlying neutral elements and molecules. Since they do not appear to generate any fluorescent lines, we will not consider these further at this time.

The hydrogen Balmer lines have full base widths ~ 100 km s^{-1}, essentially the same for all members of the series that can be measured (although above H13 or so the accuracy with which this can be determined decreases significantly due to the overwhelming effect of overlying absorption, especially early in the cycle). They are probably formed either by recombination behind the shock front or possibly by radiative excitation ahead of the shock.

Many of the Balmer lines have irregular profiles due to overlying absorption by neutral elements and molecules (see, e.g., Joy 1948). Some of these absorptions appear to give rise to weak fluorescent emission lines. In some cases entire fluorescent multiplets can be seen, indicating that some redistribution between levels is taking place.

The fluorescent lines all arise in a cooler less dense region ahead of the shock. They arise only from lower levels which are well populated at a low temperature, and this means that the lower level is either the ground state of the atom or an excited level which is already overpopulated due to another pumping process. Although there could be a region behind the shock front which is cool and tenuous enough, due to postshock refrigeration effects (see, e.g., Hill 1972), for the fluorescent lines to be formed there the sign of the velocity shifts for verified fluorescent processes rules this possibility out.

The strongest pumped emission lines are λλ4202 and 4308 of Fe I multiplet (42), and λ3852 of Fe I multiplet (73). These are excited by Mg II λ2795. As was discussed in Willson (1972), as a result of this process the $a\ ^3F_{3,4}$ levels of Fe I become overpopulated. This in turn leads to further fluorescent lines. An energy level diagram for selected levels of Fe I is shown in Figure 1, with fluorescent processes presumed present and some observed emission lines indicated. The two complex groups of multiplets which are represented, multiplets (41)–(45) and (72)–(74), have altogether seven fluorescent processes which may be acting; the same complexity is found also for Mn I and Co I.

In the same class of fluorescent lines are those pumped by Mg II λ2802, Fe II, Ti II, and Ca II K. Note that although the stellar spectrum we see has no evidence of Ca II H and K emission, only very broad absorption in those regions, the presence of Sc I (8) λ3907 indicates that Ca II K is in emission as seen by Sc I in the atmosphere.

All of the lines in this category in Table 1 which are definitely pumped require positive velocity differences between the region producing the primary line and the region containing the fluorescing atom. Although a fairly wide range of Δv's are present, the peak in number of lines and intensity of lines occurs around $\Delta v = 60$ km s^{-1}. Also among the strongest lines there is a slight tendency for the lines requiring the largest Δv's to reach their maximum intensity earlier in the cycle.

Those fluorescent lines which are excited by hydrogen may be helpful in fixing the origin of the broad hydrogen lines. The two lines which are definitely enhanced (in Table 1C[*b*]) have $\Delta v = -2$ and -14 km s^{-1}. If this indicates that the region producing the H emission is moving away from the region where these fluorescent lines are formed, then it is also a strong argument for both being formed on the same side of the shock, presumably ahead of it. This interpretation, however, fails to explain (*a*) the widths of the hydrogen lines and (*b*) how they can be excited ahead of the shock. The sample of two lines may be too small, and the implied negative Δv illusory. However, a large number of lines with positive Δv's from hydrogen lines were checked, none of which were definitely enhanced. Ultimately, a detailed consideration of shock structure will be necessary in order to establish finally where and how the hydrogen lines are formed.

We can summarize the classes of emission lines as follows:

1. Primary lines, formed in the hot post-shock region: ultraviolet lines of Mg II, Fe II, Ti II; Ca II H and K (presumed although not seen directly).

2. Hydrogen and hydrogen-like lines: H Balmer series, Si I λλ4103, 3905; Mg I λλ3829, 3832, 3838; Fe I multiplets (2), (3), (4).

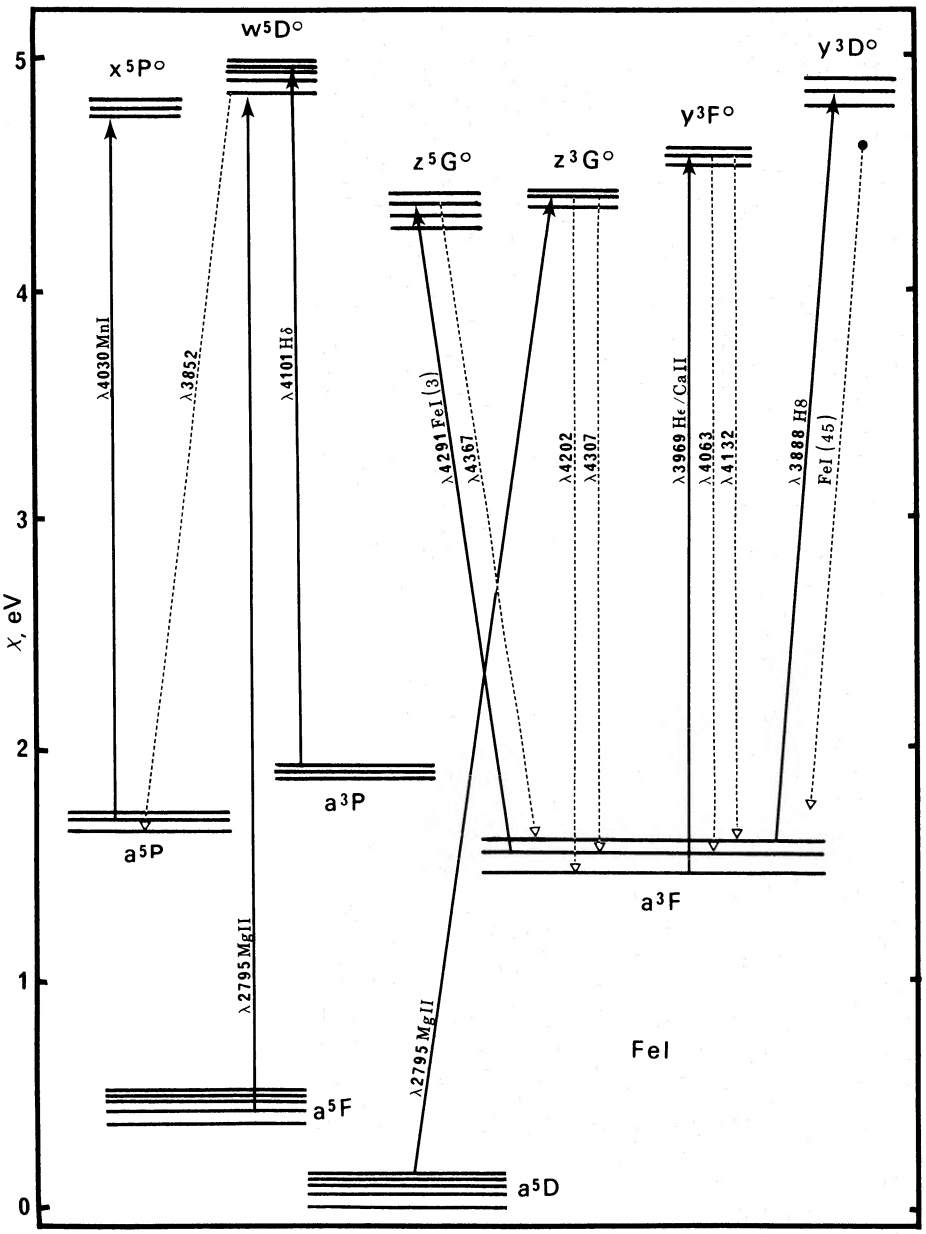

FIG. 1.—Fe I energy levels with multiple pumping processes. Solid arrows are probable pumped transitions; dotted lines are some of the more important emission lines which are observed in LPV spectra.

3. Fluorescent lines: (*a*) Fe I λλ4202, 4308, 3852; λ3936 of Co I (?); λ3907 of Sc I; λλ4030, 4033, 4034 of Mn I. $\Delta v = 0$ to $+100$ km s^{-1}; (*b*) weaker lines, pumped by (2) above: V I λ3844, In I λ4511, Fe I λ4294. $\Delta v = 0$ to -15 km s^{-1}. No lines are definitely observed to be pumped by other fluorescent lines, although several possible cases exist.

Each class of lines gives us information about the temperature, velocity, and radiation field in a different part of the atmosphere—group 1 for the region immediately behind the shock; group 2 either for a region just ahead of the shock or considerably behind it; group 3 for the cool, tenuous gas ahead of the shock.

III. DERIVING THE SHOCK VELOCITY FROM THE EMISSION LINES

The emission lines contain three distinct sources of information on the velocity field: their widths reflect, or give an upper limit to, the flow velocity where they are formed; the presence of the fluorescent lines requires definite

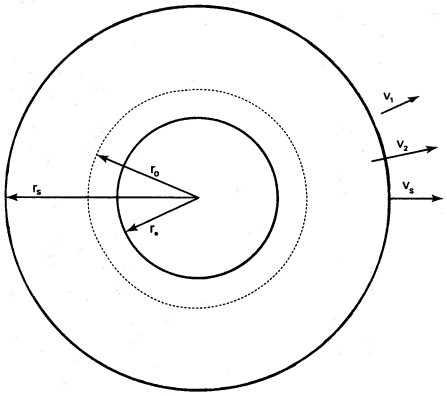

FIG. 2.—Schematic model for shock wave. Parameters are: r_* = radius of "opaque" star; r_0 = position of shock at $t = 0$; r_s = position of shock at later time t; v_s = velocity of shock relative to star; v_1 = velocity of material ahead of shock; $v_2 = v_1 + \Delta v$ = velocity of material behind shock.

velocity differences between parts of the envelopes; the emission lines are also displaced relative to the absorption lines, and this shift is a function of phase.

The line shifts have been known and analyzed for many years (see, e.g., Joy 1954); currently information is available for photospheric absorption lines, emission lines, OH, H_2O, and SiO maser lines, and circumstellar absorption (Wallerstein 1975). These data are hard to interpret in terms of a model, since (*a*) geometric effects influence the relation between line shift and actual velocity and (*b*) the velocity of the star is generally unknown. Here we will concentrate on information contained in line widths and in the fluorescent lines.

The widths of lines as a function of time, class, and excitation potential tell us of the space and time variations of the velocity. They give good upper limits on the velocity at each point, but do not give an absolute number, since both geometric effects and other broadening mechanisms may be present. Thus the shock velocity which will produce a given width and displacement for a given spectral line depends on the model, and on parameters of the model whose values may not be known. If the hydrogen lines are assumed to be due to the outward velocity of the shock region, then the shock velocity is $v = kW_H$, where W_H is some measure of the hydrogen line widths and k is a constant on the order of 1. If W_H is measured to give an upper limit, i.e., the total width at the base of the line, then $k \leq 1$. If the lines are formed ahead of the shock, such a simple relation need not hold, although the changing width of the hydrogen lines still may reflect a change in the velocity of the shock. The simplest possible model, demonstrating the geometric effects, is shown schematically in Figure 2. The light reaching us from the shell at r_s comes predominantly from the side of the star nearest us; however, if r_s is much larger than the size of the "opaque" star, r_*, significant amounts of light from the back side of the envelope will get through. Very roughly, the profile will extend from $-v$ to $+v\sqrt{[1 - (r_*/r_s)^2]}$, and thus we will have

$$\text{Width} \sim v\{1 + \sqrt{[1 - (r_*/r_s)^2]}\} \text{ at the base},$$
$$\text{Shift} \lesssim \tfrac{1}{2}v\{1 - \sqrt{[1 - (r_*/r_s)^2]}\}. \quad (2)$$

For the purely geometric model, then, $v = CW$, where W is the total base width of the line and C is between 0.5 and 1.0. The ratio of line shift to width gives a measure of the relative size of the region producing the line and the "opaque" star:

$$\frac{\text{shift}}{W} = \frac{1}{2}\,\frac{1 - \sqrt{[1 - (r_*/r_s)^2]}}{1 + \sqrt{[1 - (r_*/r_s)^2]}}. \quad (3)$$

For the hydrogen lines in R Leo this ratio is approximately 15/100; this implies $r_s \approx 1.2\, r_*$ in this simple model. That means in turn $v = CW_H$ with $C = 0.65$.

Table 2 lists maximized line widths for representative lines in the spectrum of Mira, R Leo, and R Aql. These line widths are full base widths of emission features which have been enlarged to compensate for the effects of absorption on the wings—they are thus strict upper limits on the intrinsic line widths. (Instrumental widths are estimated from comparison Fe I lines to be no more than 15 km s^{-1}; this has not been subtracted.) In a few cases trends with time are apparent; these have been noted. In all cases there is little difference from star to star; thus the assumption that these stars have comparable masses, radii, etc., should be reasonable. Within each group, lines are listed in order of decreasing average width.

The fluorescent lines which are present can be analyzed in terms of the wavelength shifts they require to give information on the "most probable velocity difference" between the regions producing the exciting line and the resulting fluorescent line. Each subclass of fluorescent lines must be considered separately in this analysis if the

TABLE 2

REPRESENTATIVE AVERAGE FULL BASE LINE WIDTHS (km s^{-1})

Star	Mira				R Leonis			R Aquilae	Trend	Average
Phase (days)	+30^d	+47^d	+55^d	+75^d	+4^d	+39^d	+39^d			
Plate No.	Ce2115[2]	Ce2188[2]	Ce2133[1]	Ce2423[2]	Pb 12758	Ce21793	Ce21798	Ce 7498		
A. Hydrogen Balmer lines	98	95	101	89	108	78	78	103	dec	94
Si I	54	53	64	66	65	54	56	64	?	60
Mg I	48	...	57	41	59	41	49	52	?	50
Fe I (2), (3)	...	40	42	...	49	46	39	44	?	43
B. Fe I λλ4202, 4307	53	58	49	...	64	53	42	46	dec	63
Fe I λ3852	20	34	58	57	35	39	40	37	?	52
Sc I λ3907	...	...	38	42	40	45	50	44	?	43
Mn I λλ4030, 4033, 4034	58	56	74	...	61	59	65	66	?	40
C. Subsidiary members of pumped multiplets:										
Fe I (42), (43) emission	...	15	$\lesssim$15	...	$\lesssim$22	16	16	$\leq$20	...	$<$17
Emission + absorption	...	35	40	...	53	41	41	38	...	$\sim$40

results are to have any physical reality. The lines in § *b* of Table 1C show small wavelength shifts, possibly implying that both exciting line and pumped line were formed on the same side of the shock. In order to obtain information on the velocity discontinuity across the shock, then, we must consider the lines in § *a* of Table 1C, the strong lines pumped by Mg II, Ca II, Fe II, and Ti II.

Joy (1948) lists the most prominent emission lines in Mira and indicates when they first appear, reach maximum and disappear during the cycle. Bearing in mind that much of their behavior is probably dependent on other parameters such as the optical depth above the shock, the strength of the exciter, and the population of the lower level of the pumped line, we can try to sift out in some simple way the velocity information they contain. Figure 3 shows an example of such an analysis. Assume that when the intensity of the line is strongest, the wavelength of the exciting line in the frame of the pumped atom must be close to what is required—we define "close" arbitrarily as within ± 30 km s^{-1}. When the line becomes weaker, it *may* be due to the absorption by the pumped atom being shifted off the peak of the exciting line. Thus we must increase our "error bars" as the line becomes fainter. Again

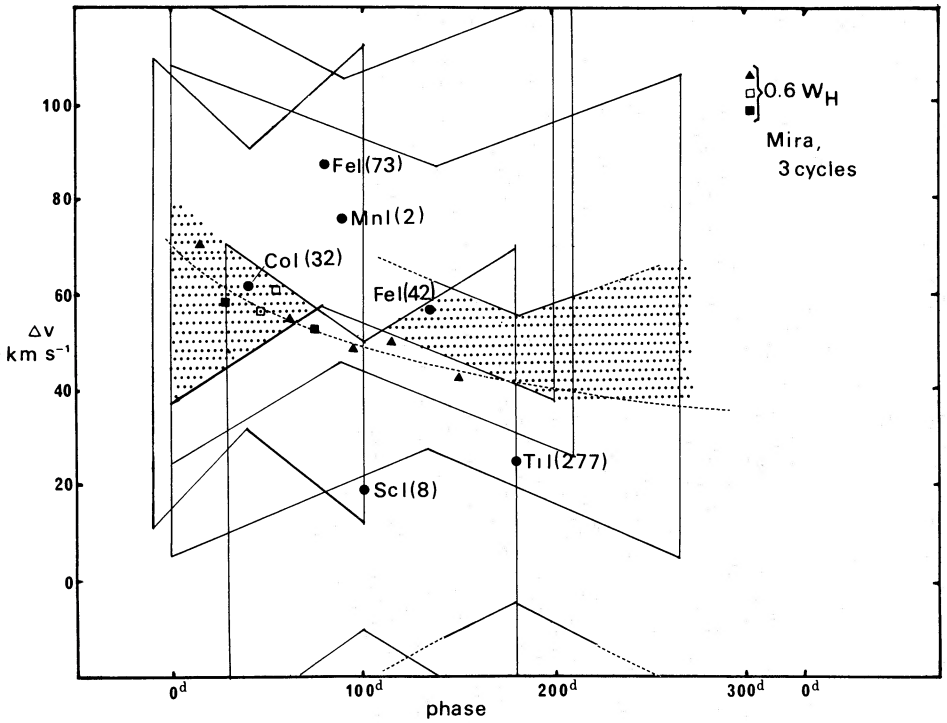

FIG. 3.—Velocity/phase analysis for Mira. Shaded region is most probable velocity discontinuity across the shock. Dashed curve is $v = 70\,(r/6\cdot 10^{13})^{-1}$ km s^{-1}.

TABLE 3

MODEL PARAMETERS WHICH WILL REPRODUCE THE HYDROGEN LINE WIDTHS AS A FUNCTION OF TIME

α	r_0 (cm)	Model
0	...	Plane-parallel atmosphere, constant velocity
1/2	1.5×10^{13}	Gravitationally decelerated shock
1	6.0×10^{13}	Spherical shock, thickness determined by recombination
3/2	2.0×10^{14}	Spherical explosion, uniform energy distribution inside
2	2.0×10^{14}	Spherical periodic model, "small orbits," and no net mass loss

arbitrarily, this means ± 50 km s^{-1} at appearance and disappearance. The result of all this is a butterfly-shaped "error box" around the point given by the ideal shift and the phase of line maximum in a diagram of Δv versus phase (Fig. 3). When all the known lines in § *a* of Table 1C are plotted this way, one region of the diagram is found to be within all the butterfly regions, i.e., to be consistent with these assumptions for *all* the lines considered. This region is shaded in Figure 3. It lies at roughly 40–80 km s^{-1} with some slight tendency toward lower velocities late in the cycle. This then implies that the probable velocity discontinuity across the shock is 40–80 km s^{-1} and decreasing.

Now, we can return to the analysis of line widths. If we assume that the hydrogen lines somehow reflect the shock velocity, so that $v = CW_H$, then the analysis of the fluorescent lines given above establishes C. The points plotted on Figure 3 are average Balmer line widths at different phases multiplied by 0.6; as is evident in the figure, these points fall nicely in the region of "most probable velocity." This number is certainly consistent with the value 0.65 derived from purely geometric considerations above!

Note that although the material behind the shock will not be moving outward with the shock front velocity, since the shock moves through the material, the difference is at most the speed of sound behind the shock—which is at most 10 km s^{-1}. To within the accuracy of these measurements, it is sufficient to assume they are the same. Thus we assume $v_s \approx \Delta v \approx v_2$ in all that follows.

The hydrogen line widths are essentially independent of excitation potential of the upper level, although the higher members of the series are harder to measure accurately. They show a gentle decrease with time, consistent with a power law

$$v = v_0(r/r_0)^{-\alpha}, \tag{4}$$

where several (α, r_0) pairs are possible; $v_0 \approx 70$ km s^{-1} for all of these. Table 3 summarizes the possible combinations of r_0 and α, with reference to the sort of model which will produce each α. Values of r_0 greater than 5×10^{13} seem most likely. This is quite reasonable: for R Leo, with the same line widths, the measured diameter is 16 AU, or $r \approx 10^{14}$ cm (Nather and Wild 1973). The parameters r_0, v_0 are here interpreted to mean the size and speed of the shock front at maximum light.

The next step in the analysis is to compare these results with theoretical models, to see if they can be interpreted in a way which makes physical sense. That is the subject of the next section.

IV. THE SHOCK VELOCITY MODELS

In this section we explore some simple models with the goal of understanding and interpreting the observed emission-line velocities and intensities. Specifically, we seek the velocity discontinuity across the shock, Δv, as a function of r or t.

For a plane-parallel atmosphere for RR Lyrae stars Hill (1972) found that when a "steady state" had been reached, Δv, the velocity discontinuity across the shock, was constant. This may be derived from two simple assumptions for the plane-parallel case: that the flow is strictly periodic, so at a given r the velocity of flow into the shock is the same for every cycle; and that the shock imparts a velocity v_0 to the gas which is subsequently affected only by gravity, neglecting, e.g., pressure effects. (Note that the plane-parallel assumption implies also that the net outflow is negligible.) Then at time t

$$v = v_0 - gt. \tag{5}$$

In order for the velocity to return to its original preshock value at $(r, t + P)$, $\Delta v \approx gP \approx$ constant, where P is the period.

For the spherical case, g is no longer constant, and thus for strict periodicity, assuming there is no net outflow and the "orbit" of a single gas particle is small compared with r,

$$\Delta v = gP \propto 1/r^2. \tag{6}$$

This is the $\alpha = 2$ case of Table 3, which best fitted the observations when $r_0 = 2 \times 10^{14}$ cm. This leads to a contradiction: if $\Delta v \geq 30$ km s^{-1} with $P = 3 \times 10^7$ s, then $g \geq 0.1$ is required for $\Delta v = gP$. However, with a mass of

$\lesssim 1\ M_\odot$ (see Fernie and Brooker 1961) and $r \approx 2 \times 10^{14}$ cm, $g = GM/r^2 \lesssim 2 \times 10^{-3}$. To get $g \geq 0.1$ with $M \sim 1\ M_\odot$ requires $r \lesssim 2 \times 10^{13}$ cm; but this does not fit the hydrogen line widths for $\alpha > \frac{1}{2}$. The resolution of this apparent conflict is simple: with the large velocities observed, particle orbits in a period are large compared with r—in fact, the particles are probably not bound, and there is net outflow.

Allowing for large orbits or a net outflow of matter in the spherical case can be done by expressing Hill's results differently. For a strong shock the velocity can be written in terms of the net energy as

$$\Delta v \approx \left(\frac{E}{\frac{1}{2}\rho \text{ volume}}\right)^{1/2} . \tag{7}$$

For the plane-parallel case, the volume is proportional to Δr, where Δr is the effective thickness of the region containing most of the shock energy. This thickness may be estimated as the distance which hydrogen ions travel behind the shock before recombining and radiating away their excess energy:

$$\Delta r \approx v_s t_{\text{rec}} \approx \frac{v_s}{\rho}\left(\frac{\mu m_{\text{H}}}{\alpha_{\text{rec}}}\right) . \tag{8}$$

Thus $\rho \Delta r \propto v_s \approx \Delta v$, so we can summarize Hill's result for the plane-parallel shock by writing

$$\Delta v \propto (E/\Delta v)^{1/2} \approx \text{constant} . \tag{9}$$

For the spherical case this generalizes very simply to

$$\Delta v \propto \left(\frac{E}{\Delta v}\frac{1}{r^2}\right)^{1/2} \propto \frac{1}{r} . \tag{10}$$

Thus the $\alpha = 1$ case is the most reasonable spherical generalization of Hill's calculations.

With this formulation we can also estimate the fraction of the total shock energy which is lost by radiation during one period:

$$\frac{E_i}{E_f} = \frac{v_i}{v_f} \approx 2 ; \tag{11}$$

or about 50 percent of the shock energy is radiated away.

Two other "models," $\alpha = \frac{1}{2}$ and $\alpha = 3/2$, are listed for completeness in Table 3. These correspond to, e.g., for $\alpha = \frac{1}{2}$ a shock decelerated gravitationally, so that $v^2 = v_0^2 - (GM/r_0)(1 - r_0/r)$; for $\alpha = 3/2$, a spherical explosion where the energy is distributed throughout a volume proportional to r^3.

The $\alpha = 1$ model is to be preferred, for two reasons. First, it is the most easily justified generalization of Hill's results. Second, it gives a value for r_0 close to the observed radius of R Leo at maximum, 10^{14} cm. Note that $r_0 \approx 10^{14}$ is also indicated as a scale by the shock velocity: $v_0 P \approx 2 \times 10^{14}$ cm.

V. SOME CONSEQUENCES OF THE LARGE SHOCK VELOCITY

Once the shock velocity and conditions ahead of the shock are known one can in principle determine the density, temperature, pressure, and ionization equilibrium behind the shock, the thickness of the radiating postshock region, and the total luminosity of the shock. In practice some of these require lengthy calculations and will therefore not be discussed here. However, a few consequences of the large velocity discontinuity indicated by the fluorescent lines should be mentioned.

Note that the quantity determined from the fluorescent lines is the velocity discontinuity, not the actual shock velocity with respect to the star. The material ahead of the shock may be falling in toward the star; then $v = \Delta v - v_1$ is less than Δv. Also recall that the material behind the shock moves at v_2 which may be as much as 10 km s^{-1} slower than the shock front velocity. Tsuji (1971) suggested on the basis of circumstellar features that the material is flowing outward at $\sim$20 km s^{-1}; there is nothing here that contradicts that result. On the other hand, the fluorescent lines give a *lower* limit on the actual velocity discontinuity across the shock, since the material behind the shock may slow down considerably before radiating. Also, if the material ahead of the shock is already flowing outward, then the shock velocity may be larger than the measured Δv. Resolution of this question must come from observations of stars with known radial velocity and/or from detailed models of the evolution of the shock-influenced atmosphere.

A velocity discontinuity of 50 km s^{-1} is very large. The speed of sound at $T < 10^4$ is $\lesssim$10 km s^{-1}, so the shock is moderately strong. The velocity of escape from a $1\ M_\odot$ star with $r \approx 10^{14}$ cm is 16 km s^{-1}, so the material in the shock is probably unbound and will escape to infinity. Thus a significant amount of shock driven mass loss is suggested, apart from any other mass loss processes that may be operating. This large a velocity also implies that a considerable fraction of the energy output of the star is the mechanical energy of the shock, and that this is probably very important in determining the atmospheric structure.

In a reference frame moving with the shock, material enters the shock at density ρ_1, velocity u_1, and leaves with ρ_2 at velocity u_2. For a shock with large Δv, u_1 is much larger than the speed of sound in the medium ahead of the shock, c_1, and $u_2 \ll c_2$. Thus the shock equations simplify to

$$\rho_1 u_1 = \rho_2 u_2 = M\,, \tag{12a}$$

$$P_2 \approx \rho_1 u_1^2\,, \tag{12b}$$

$$\int Q dx \approx \tfrac{1}{2}\rho_1 u_1^3 + \epsilon_2 \frac{M\chi}{m_{\rm H}}\,, \tag{12c}$$

where Q is the radiation rate from a unit volume and ϵ_2 is the fractional ionization behind the shock (see, e.g., Whitney and Skalafuris 1963). Equation (12a) may be rewritten in terms of Δv and the speed of sound behind the shock as

$$\rho_2/\rho_1 \gtrsim \Delta v/c_2\,, \tag{13}$$

which is at least 5 from the observed velocities alone. Alternately, for a strong shock

$$\frac{\rho_2}{\rho_1} \approx \frac{\gamma + 1}{\gamma - 1}\,, \tag{14}$$

which is 4 for an ideal gas with no shock-induced ionization and ~ 10 or higher if ionization is taking place (see, e.g., Zel'dovich and Raizer 1967, Vol. **1**, p. 94). Thus the velocities observed are consistent with a strong, ionizing shock.

We can use (12c) to estimate the luminosity of the shock; assuming $\rho_1 \approx 10^{-12}$ g cm^{-3} and $\Delta v \approx u_1$,

$$L_{\rm shock} \lesssim \tfrac{1}{2}\rho_1 u_1^3 4\pi r^2 \lesssim 10^{37} \text{ ergs s}^{-1}\,, \tag{15}$$

where the upper limit on L is obtained by neglecting the energy left as ionization and thermal energy. Note that the luminosity of a long-period variable at maximum is of this order also (see, e.g., Allen 1973)—thus the energy and luminosity of the shock are important.

The luminosity of the shock is equal to 10^{37} ergs s^{-1} if *all* the energy is lost through radiation from the ionized region. However, this is obviously not the case—some of the energy presumably goes into heating the postshock photosphere from 2000 K to 2500 K. This may be taken into account as follows:

Following Ledoux and Walraven (1958, p. 561), we write

$$\frac{T_2}{T_1} = \frac{P_2}{P_1}\frac{(1 + X_1)}{(1 + X_2)}\frac{(2\chi_{\rm H}/m_{\rm H}\tau_1)(X_1 - X_2) + P_2 + 4P_1 + 2(F_1 - F_2)/\Delta m\tau_1}{4P_2 + P_1}\,, \tag{16}$$

where X_1 is the fraction of the hydrogen ahead of the shock which is ionized, $\tau_1 = 1/\rho_1$, $\Delta m = \rho_1 u_1$, F_1 is the radiation from ahead of the shock to behind, and parameters with subscripts 2 are for the region behind the shock.

Assume that at some time past the shock the radiation F_2 has been emitted, any hydrogen ionized in the shock has recombined, and we are left with a neutral gas at T_2. Using the ideal gas law and neglecting P_1 and F_1, we find from (16)

$$F_2 = \frac{k}{2m_{\rm H}}\left(\frac{\rho_2}{\rho_1} - 4\right)\Delta m T_2\,. \tag{17}$$

If we assume that $\rho_2/\rho_1 \approx 10$, and substitute $N_1 = \rho_1/m_{\rm H} = 10^{12}$ cm^{-3}, $u_1 \approx 5 \times 10^6$ cm s^{-1}, and $T_2 \approx 2500$ K, we find $F_2 \approx 5 \times 10^6$ ergs cm^{-2} s^{-1}. This implies a total luminosity for the ionized region behind the shock of $\sim 5 \times 10^{35}$ ergs s^{-1}—or a few percent of the net luminosity at maximum should be in the form of recombination lines, the rest emerging as increased $T_{\rm eff}$. Again, a detailed calculation of shock structure and ionization balance is required to predict the postshock temperature; here we have assumed a value consistent with observations and shown that it results in a reasonable shock luminosity.

A large shock velocity also has implications for the atmospheric structure. Hill (1972) noted that for the periodic solution discussed in § IV, scale height of the RR Lyrae atmosphere was extended by a factor of 20 or so. This can also be easily checked for the long-period variables. Write

$$\frac{h}{H} = \frac{mgh}{kT} \rightarrow \frac{mgh}{kT + \text{Kinetic Energy}} = \frac{h}{H'}\,. \tag{18}$$

Then

$$H' = \frac{kT + \tfrac{1}{2}mv^2}{mg} = \left(\frac{kT + \tfrac{1}{2}mv^2}{mGM}\right)r^2\,, \tag{19}$$

where m is the mean molecular mass $\mu m_{\rm H}$. For the unperturbed atmosphere using $M \approx 10^{33}$ g and $m \approx m_{\rm H}$, the scale height is

$$H \approx 10^{11} R^2\,(\mathrm{AU})/M(_\odot)\,, \tag{20}$$

which is 1 percent of R if $R = 10^{13}$ cm and 10 percent of R if $R = 10^{14}$ cm. Thus for the unshocked atmosphere, spherical effects are not necessarily large. Taking into account the dynamics, however, using $v \approx 50$ km s^{-1} gives H' larger by a factor of 10:

$$H' \approx 10^{12} R^2\,(\mathrm{AU})/M(_\odot)\,. \tag{21}$$

This is $H' \approx R$ for $R = 10^{14}$: spherical effects *are* important.

VI. SUMMARY

From an analysis of the fluorescent emission lines in the spectra of long-period variable stars, limits on the velocity discontinuity across the shock of 40 km s$^{-1} \leq \Delta v \leq 80$ km s^{-1} can be found. From an independent analysis using the widths of the hydrogen Balmer lines, it is deduced that the shock velocity decays as $(r/r_*)^{-1}$. Putting these together, we found

$$v \approx 70(r/10^{14}\ \mathrm{cm})^{-1}\ \mathrm{km\ s^{-1}}\,. \tag{22}$$

This high velocity then led us to conclude that the mechanical energy of the shock is dominant in determining the atmospheric structure, that the shock contributes significantly to the luminosity of the star, and finally that as a result, spherical symmetry is important for these atmospheres.

My deepest gratitude to G. Wallerstein who provided both the observational material for this paper and the opportunity to work on it during a beautiful Seattle summer. Thanks are also in order for B. Peery, H. R. Johnson, and numerous others for suggestions and criticisms in the early stages. This work was supported in part by NSF grant GP-28882.

REFERENCES

Allen, C. W. 1973, *Astrophysical Quantities* (3d ed.; London: Athlone Press).
Fernie, J. D., and Brooker, A. A. 1961, *Ap. J.*, **133**, 1088.
Hill, S. J. 1972, *Ap. J.*, **178**, 793.
Joy, A. H. 1948, *Ap. J.*, **106**, 288.
———. 1954, *Ap. J. Suppl.*, **1**, 39.
Kondo, Y., Giuli, R. T., Modisette, J. L., and Rydgren, A. E. 1972, *Ap. J.*, **176**, 153.
Ledoux, P., and Walraven, Th. 1958, *Handbuch der Physik*, ed. S. Flügge (Berlin: Springer-Verlag), **51**, 554.
Meinel, A. B., Aveni, A. A., and Stockton, M. W. 1969, *Catalogue of Emission Lines in Astrophysical Objects* (Tucson: University of Arizona).
Merrill, P. W. 1947, *Ap. J.*, **106**, 274.
Moos, H. W., Linsky, J. L., Henry, R. C., and McClintock, W. 1974, *Ap. J.* (*Letters*), **188**, L93.
Nather, R. E., and Wild, P. A. T. 1973, *A. J.*, **78**, 628.
Tsuji, T. 1971, *Pub. Astr. Soc. Japan*, **23**, 275.
Wallerstein, G. 1975, *Ap. J. Suppl.*, No. 291, **29**, 375.
Whitney, C. A., and Skalafuris, A. J. 1963, *Ap. J.*, **138**, 200.
Willson, L. A. 1972, *Astr. and Ap.*, **17**, 354.
Zel'dovich, Ya. B., and Raizer, Yu. P. 1967, *Physics of Shock Waves and High Temperature Hydrodynamic Phenomena* (New York: Academic Press), Vols. **1** and **2**.

LEE ANNE WILLSON: Erwin W. Fick Observatory, Physics Department, Iowa State University, Ames, IA 50010